THE JOURNAL OF PHYSICAL CHEMISTRY C

Article

pubs.acs.org/JPCC

Analysis of Anhydrous and Hydrated Surface Energies of gamma-Al_2O_3 by Water Adsorption Microcalorimetry

Ricardo H. R. Castro* and Dat V. Quach

Peter A. Rock Thermochemistry Laboratory and NEAT ORU, University of California, Davis, One Shields Avenue, Davis, California 95616, United States

ABSTRACT: Surface energies have postulated importance to catalysis, crystal growth, sintering, polymorphism, and many other fields. This importance is even more critical when dealing with nanostructured materials, where the surface-to-volume ratio is considerably higher and the surface term accounts for a much larger fraction of the total free energy. Here we present a novel approach to experimentally assess the average anhydrous and hydrated surface energies of oxides, and used the method to determine the surface energy of gamma-alumina. The method uses a water adsorption setup combined with a microcalorimeter where the heat of adsorption can be monitored as a function of the adsorbed amount. Maintaining a closed system, the approach enables the correlation of the molecular configuration of absorbed water with the thermodynamic data, and hence the definition of the point where a liquid water configuration exists (at high relative humidity). This information allows the calculation of the surface energy at room temperature for any coverage state by using the adsorption calorimetric data. For gamma-alumina, a close relationship between the water adsorption behavior and the surface energy was observed, evidencing that higher surface energies are associated with highly energetic dissociative behaviors of water and a continuous surface energy decrease upon water adsorption. Three adsorption stages were clearly observed from the combination of adsorption isotherm and microcalorimetric data, consistently with presented models.

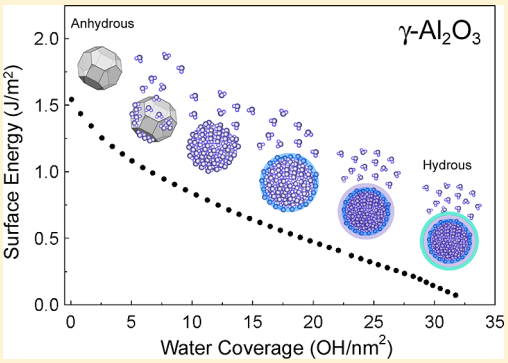

1. INTRODUCTION

Surface energies are directly related to the driving forces of important phenomena for micro- and nanostructured control, such as coarsening, sintering, and polymorphic stability. Therefore, the knowledge of those energies can be used not only to better understand but also to improve the control of those phenomena on a thermodynamics basis. However, while in liquids the measurements of surface tensions have been well understood and widely exploited, solid surface energies, in particular for nanocrystalline oxides, are difficult to experimentally assess, and reliable data for both anhydrous and hydrous surfaces are not largely available, especially for multicomponent systems.[1−7]

The measurement of surface energies in solids has been a classical problem for many years, and interesting and elegant solutions have been proposed.[8−12] While surface energies can be derived from measurements of the elastic modulus of submicrometer powders,[8] or by wetting contact angles,[11] room temperature anhydrous surface energies data for nanomaterials have only been recently reported by using a calorimetric approach.[12−14] This last one is mostly based on the measurement of the heat of high temperature oxide melt solution of a series of samples of a given composition and structure but with distinct surface areas. The method assumes that the heat of solution will have a linear dependence on the surface area, and that the slope is directly related to the surface energy.[12] Since this calorimetric procedure is performed on nanomaterials, the data typically require corrections for water adsorption by using thermochemical cycles, which is done by combining the drop solution calorimetry with a microcalorimetry analysis of water adsorption.[13−15] A significant limitation of the approach is that samples with different surface areas are required to have similar shapes, and consequently similar crystallographic planes exposed on their surfaces, in order to hold the linear dependence between the heat of drop solution and surface area. This is not an obvious condition for nanostructures such as TiO_2 nanocrystals, where the effect of edges and defects significantly affects the average surface energies below a critical size.[16] The other fundamental limitation of this technique emerges when studying doped samples. Since the specimens with different surface areas are typically prepared by systematic thermal treatments to promote coarsening, a redistribution of the dopants along the sample is likely to occur. This may cause heterogeneities among them and, consequently, result in a nonlinear dependence of the enthalpy of drop solution on the surface area.[17,18]

In this paper, we present an alternative approach to determine both anhydrous and hydrated surface energies of nanocrystalline oxides based on a thermodynamic analysis of water adsorption. The method requires a single set of samples (i.e., with a single surface area) and provides representative data on the average energy of the surfaces present in the studied

Received: September 19, 2012
Revised: October 30, 2012
Published: November 5, 2012

   dx.doi.org/10.1021/jp309319j | J. Phys. Chem. C 2012, 116, 24726−24733

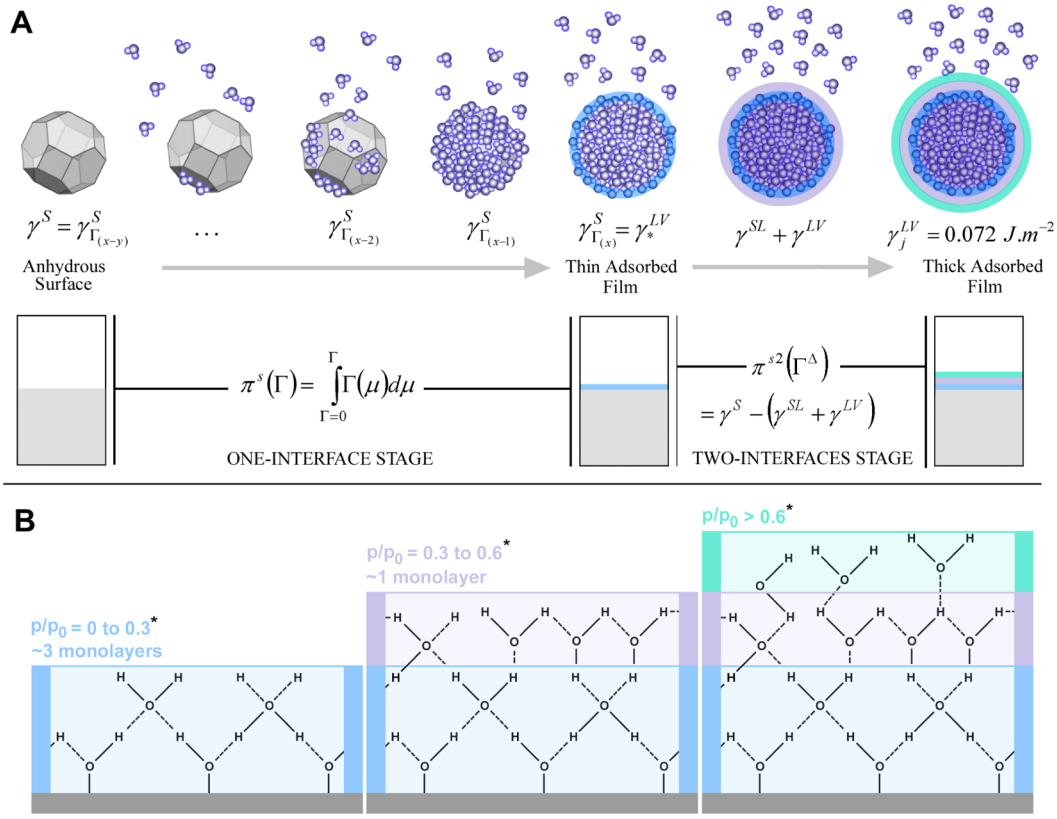

Figure 1. Schematic representation of the adsorption process of water on the surface of a particle. Part A shows the two-stage adsorption behavior, with the formation of a thick film after a critical coverage of the surface. Each stage should be treated with a different equation, as shown in the figure. Part B shows how the adsorption happens at the molecular scale, showing the dissociative behavior, followed by a transitional stage, and the liquid-like stage. The numbers of monolayers and pressures (indicated with an asterisk) are for silicon dioxide from ref 24.

specimen. The instrumentation requirements are not exceedingly complex, and the approach is adequate for multicomponent systems, where thermal treatments can affect the nature of the samples.

Using the proposed method, we studied the surface energy of gamma-alumina and its dependence on the water adsorption. Gamma-alumina is an important base material for a variety of catalysts, and its surface energy is of prime importance to predict stability as well as reactivity under different environments during processing or operation.[12,13] We have measured the surface energy of gamma-alumina nanoparticles with the proposed method at different water coverages, and observed a clear inverse relationship between the enthalpy of adsorption and the actual surface energy; i.e., more negative enthalpies of adsorption correspond to higher surface energies.

1.1. Water Adsorption Theoretical Background. The thermodynamics of vapor adsorption on a solid surface has been closely related to wettability and even to relative surface energies,[19−23] but a direct measurement of anhydrous surface energies from vapor adsorption has not been shown theoretically or experimentally.[21] In a typical water adsorption experiment, the solid is dried in a vacuum chamber and then exposed to small controlled dosages of vapor. Adsorption then results in reversible formation of a layer or film on the surface of the solid and leads to a decrease in the surface tension. The problem of adsorption is typically discussed using Gibbs adsorption equation:[20]

$$d\gamma = -S_a^\sigma\, dT - \sum_i \Gamma_i\, d\mu \qquad (1)$$

where S_a^σ is the excess entropy of the surface per unit area, γ is the surface energy, T is the temperature, μ is the chemical potential, and Γ_i is the excess adsorbed amount of component i per total surface area. For pure vapor adsorption (one component) at constant temperature on an insoluble nonvolatile solid, the adsorption equation only contains the excess term on the right of eq 1. Integrating from the anhydrous state, we have

$$\pi^s(\Gamma) = \int_{\Gamma=0}^{\Gamma} \Gamma(\mu)\, d\mu \qquad (2)$$

where π^s is the difference between the surface energy of the clean (anhydrous) solid surface, denoted by γ_0^S, and the surface energy γ_Γ^S of the same surface after adsorption of the excess Γ.

Equation 2 suggests that it would be possible to determine the relative surface energies if the absorbed amount is known. However, the single surface tension model does not describe the full adsorption process at high water coverage. According to Schlangen et al.[20] and Adamson,[23] the vapor adsorption process takes places in two stages, one where the surface is considered a single interface being covered by molecules and another where a thick water film is formed. While the first stage can be described by the model presented above, the second needs to address both solid−liquid and liquid−vapor interfaces.

Figure 1A illustrates how the water adsorption takes place on the surface of a solid particle. Starting from a clean surface, the adsorbed water modifies the surface energy of the solid until there is a microscopic film covering the surface. From this point

dx.doi.org/10.1021/jp309319j | J. Phys. Chem. C 2012, 116, 24726−24733

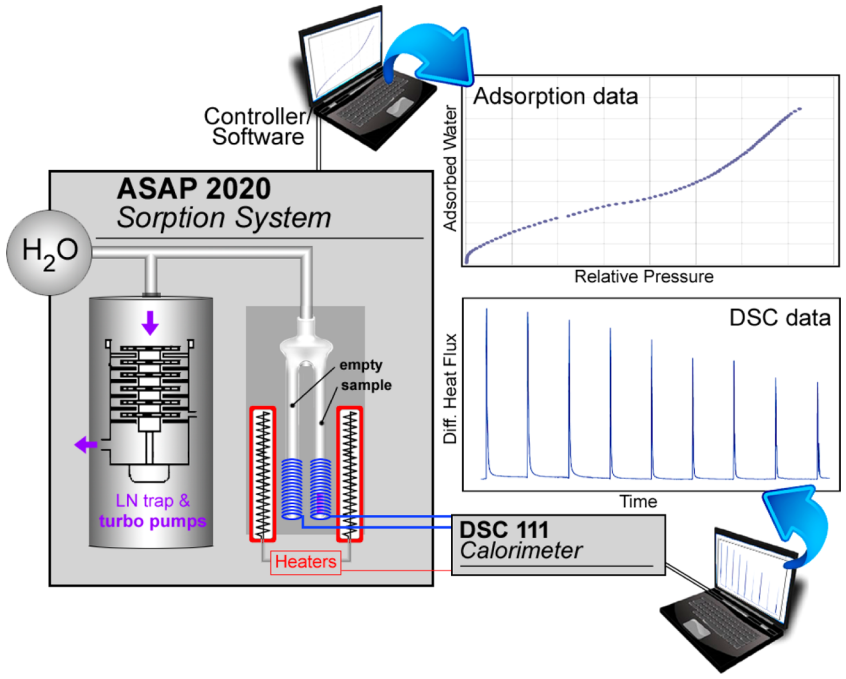

Figure 2. Schematic representation of the setup designed to measure the heat of adsorption of controlled microdosages of water vapor. A glass fork-shaped tube was manufactured and connected to the ASAP2020 Sorption System. The fork-tube allows the system to be concomitantly connected to a calorimeter. By leaving one leg of the tube empty and loading the other with the sample (typically loosely pressed pellets of the nanopowder), one can measure the differential heat exchange during the adsorption process. ASAP2020 is equipped with turbo pumps and a liquid nitrogen trap to allow full degassing of the sample. Heating is also applied to assist degassing and allow an anhydrous initial state. Data from adsorption and calorimetry are combined to determine the heat of adsorption per mole and the surface energy of the sample.

on, the energy change upon further adsorption is better described by[20]

$$\pi^{s2}(\Gamma^{\Delta}) = \gamma_0^S - (\gamma^{SL} + \gamma^{LV}) \quad (3)$$

where γ^{SL} and γ^{LV} are the solid−liquid and liquid−vapor interface energies and Γ^{Δ} represents the coverage beyond the formation of the water film. While γ^{SL} can be considered constant during the process (though unknown), γ^{LV} is expected to suffer influence from the solid−liquid interface (as the surface ordering, electrostatic, and molecular forces are affecting the liquid). This influence is strong for very thin films but decreases as the thickness increases. At certain *critical film thickness*, one may expect that the effect of the solid surface on γ^{LV} is negligible, suggesting that γ^{LV} is then exactly that of bulk water, 0.072 J·m^{-2} (72 erg·cm^{-2}).

Asay and Kim[24] provided an enlightening molecular description of the adsorption process, as shown in Figure 1B. By using sophisticated experiments on attenuated total reflection infrared (ATR-IR) spectroscopy, they showed that indeed the process of adsorption has not one but three states. When the surface is exposed to small relative humidity, water molecules are strongly attached (dissociation) to the surface and adopt a configuration significantly affected by it.

For SiO_2, for instance, the water is in an "ice-like" state that is typically three monolayers thick on the surface, and is the only coverage type up to relative humidity 30%. For higher coverage, the water assumes a transitional state. That is, the effect of the solid surface is no longer so strong, and water structure relaxes. This layer is typically only 1 monolayer thick (maybe considered an interface), and for further coverage, the water assumes a "liquid-like" state. This last state was confirmed by the vibrational peaks from the spectroscopic analysis, and was observed for SiO_2 to occur for relative humidity higher than 60%. The distinct vibrational bands for adsorbed water at different relative pressures were also very consistent with the measured profiles of adsorption isotherms, which showed clear changes in behavior (derivative) at the same relative humidity where the spectroscopy revealed a modification in the water structure.

Al-Abadleh and Grassian[25] reported a similar water behavior for aluminum oxide, showing the three different states by infrared spectroscopy and on the adsorption isotherm. The structural changes were though in slightly different relative pressures, suggesting that the surface had a different impact on the water structure. Indeed, one should expect that every oxide will have a slightly different interaction with water but following a similar general adsorption profile.

The fact that the water assumes a liquid-like structure for high relative pressures indicates that, from that point on, the surface tension is actually that of bulk water.[24] With this information, one might be tempted to use eqs 2 and 3 to calculate the surface energy of the system for lower water coverage. However, the unknowns on the solid−liquid interface energies make the problem unsolvable, enabling only relative values to be estimated.[22]

A carefully designed calorimetric experiment can provide the needed information to assess absolute values of surface energies at the anhydrous state and at any water coverage condition. The possibility of such an approach has been proposed by McHale et al.[12] when describing the very distinct heat of adsorption of gamma-alumina versus alpha-alumina. It was shown that the alpha alumina showed a much higher heat of water adsorption than gamma-alumina, and from another method (high temperature oxide melt solution calorimetry), the surface energies of these polymorphs were observed to

dx.doi.org/10.1021/jp309319j | J. Phys. Chem. C 2012, 116, 24726−24733

follow the same trend. No details were given at that occasion on how to quantitatively extract surface energies from the adsorption data, and we propose the method here for the first time.

2. EXPERIMENTAL PROCEDURES

2.1. Microcalorimetry of Adsorption. The goal of the experiment is to measure the heat of adsorption of water molecules on the surface of an oxide as a function of the relative pressures. To achieve this, we used the ASAP 2020 Micromeritics equipped with furnace and turbo-pumps for degassing. ASAP 2020 records relative pressures and adsorbed amounts for the series of adsorption, and we combined a Calvet-type microcalorimeter (Setaram DSC-111) to the analysis chamber to attain additional data on the enthalpy of adsorption.[14] Figure 2 shows a schematic representation of the setup.

The sample is placed in the analysis chamber (right leg of a fork tube in the figure) and degassed to ensure an initial anhydrous surface condition (the degassing parameters depend on each material, and need assistance from thermogravimetric experiments to ensure complete water removal). After that, the fork tube is kept at constant temperature (regulated by the calorimeter), and a small dose of water (μmol) is pumped into the system, automatically controlled by the ASAP instrumentation. The DSC records the heat flow difference between the empty leg of the fork tube and the one containing the sample, as in a regular DSC experiment.

Since the bulk of the solid is not affected by the experiment, the only existing reaction is the adsorption process, described by

$$\text{Surface} + n_{ads}H_2O_{(gas)} \Leftrightarrow \text{Surface}, n_{ads}H_2O_{(adsorbed)} \quad (4)$$

where n_{ads} is the number of adsorbed molecules. This is true only if there are no other irreversible reactions, such as formation of hydroxides as reported for MgO.[26] The combined calorimeter will record the energy of the adsorption process plus the internal heat of the water molecules being injected (that is, the calorimeter is recording from the moment that the powder is degassed on). The internal energy is however negligible, and so the measured heat can be directly attributed to eq 4.

The Gibbs free energy change associated with eq 4 at a given temperature and pressure is

$$\Delta G = G(\text{Surface}, n_{ads}H_2O_{(adsorbed)}) - G(\text{Surface}) - n_{ads}\mu_{H_2O} \quad (5)$$

where μ_{H_2O} is the chemical potential of water. If the bulk energy remains unchanged with respect to adsorption, one neglects the entropic and pV terms, and the reactions are reversible, using the same notation in eq 3, we have:

$$\gamma^S = \gamma_0^S + \theta\cdot\Delta H_{ads} \quad (6)$$

where θ is the surface coverage, ΔH_{ads} is the measured heat of adsorption (kJ.mol^{-1}), and γ^S is the surface energy at the given surface coverage. Similarly to eq 3, eq 6 establishes a relationship between two surface energies at different water coverage. However, eq 6 is more powerful, as it addresses the thermodynamics of the system without being limited by the adsorption profile. That is, since the experiment uses a closed system, the measured energy (ΔH_{ads}) during the adsorption includes any component of the adsorbed layer. While for low coverage this will only include the single adsorption with the surface, at higher coverage, it will include the effect of adsorption on the formation of the film.

As mentioned before, with increasing relative humidity, at a certain point, one expects the water molecules to be liquid-like. If this is the case, ΔH_{ads} will be that of a water molecule adsorbing on a liquid droplet. This number should be equal to the enthalpy of liquefaction of water (−44 kJ·mol^{-1}). Several works have shown that this is actually observed for water adsorption experiments, and if the studied surface is composed mostly of hydrophilic sites, the heat of adsorption achieves −44 kJ·mol^{-1} at relatively low coverage.[12,27] If the surface is hydrophobic, the heat of adsorption typically goes below (in modulus) −44 kJ·mol^{-1}, before at much higher coverage returning to it.[27] The fact that the heat of adsorption can potentially be less negative than the heat of liquefaction is counterintuitive for most, but it has been shown to be a manner to experimentally identify hydrophobic surfaces, as shown by Bolis et al.[27]

Real particles and nanoparticles are composed by different exposed surface planes. Some of them will be more hydrophilic than others, and thus, during an adsorption experiment, one should expect that the more hydrophilic sites will be filled first, followed by the more hydrophobic as the relative pressures increase. This is by no means inconsistent with the adsorption models described above, as even for hydrophobic sites, the process is still spontaneous (exothermic). Therefore, for higher coverage, the numbers will eventually converge to the heat of liquefaction.

In conducting the microcalorimetric experiment in the gamma-alumina samples, about 15 mg of powder was used, providing a total surface area of 2.79 m^2. The sample was degassed for 2 h. The chamber was kept at 25 °C, and the dosing routine was programmed to be ∼2 μmol of H_2O per dose and equilibration time ∼1 h. A correction for water adsorption on the tube and manifold was made from a blank run. The calorimeter was calibrated using the enthalpy of fusion of gallium.

2.2. Synthesis and Characterization of Gamma-Alumina. Gamma-alumina was prepared by a polymeric precursor method. Citric acid and ethylene glycol were mixed with aluminum nitrate to form a clear solution. The solution was brought to 120 °C for polyesterification and formation of metal chelates. The resin was then treated at 650 °C for 4 h, obtaining a gray powder composed of aluminum hydroxide and carbon residues. This was retreated at 800 °C for 12 h under air to transform to gamma-alumina and eliminate all carbon by combustion. Thermogravimetry and infrared spectroscopy using a Bruker Equinox 55 FTIR spectrometer for mid- and near-IR range analysis were used to test for the presence of carbonate phases and organic residues in the sample. Thermogravimetry also showed that significant mass changes can only be observed up to 750 °C; hence, this temperature was selected for degassing prior to both BET and water adsorption experiments. X-ray diffraction was performed on the studied sample using a Bruker-AXS D8 Advance diffractometer (Bruker-AXS, Inc.) operating at an accelerating voltage of 40 kV and an emission current of 40 mA with a copper target as an X-ray source.

3. RESULTS

Figure 3 shows the X-ray diffraction pattern for the as-synthesized gamma-alumina. The pattern shows the absence of

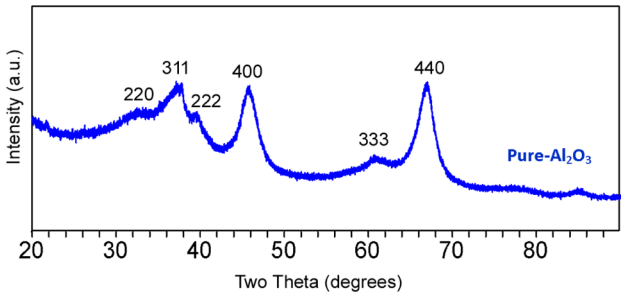

Figure 3. X-ray diffraction pattern for nanocrystalline gamma-alumina prepared by the polymeric precursor method.

alpha or hydroxide phases. Previous studies for transitional aluminas prepared from this method confirm it is gamma rather than other transitional phases such as theta or sigma.[13] Thermogravimetry and infrared spectroscopy showed the absence of any organic compounds or carbonated phases on the studied sample. N_2 adsorption (BET method) showed a surface area of 186.7 ± 3.8 $m^2 \cdot g^{-1}$ for the sample, an area significantly high for the intended microcalorimetric study. Figure 4 shows the isotherm of adsorption (coverage as a

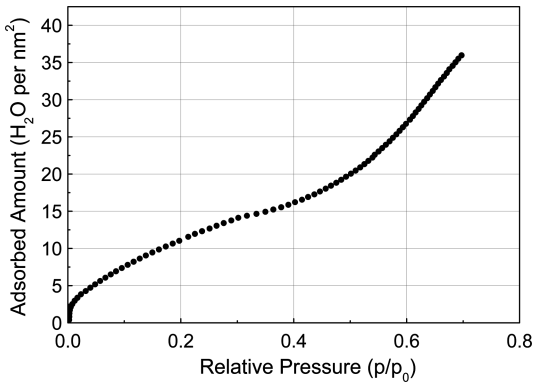

Figure 4. Adsorption isotherm of water on anhydrous gamma-alumina. The shape of the curve shows at least three clear adsorption stages. The curve was corrected for adsorption on empty tube under the same conditions.

function of relative pressure) for one of the curves used in the study (experiments were repeated to ensure consistency). The shape of the curve is consistent with previous adsorption data for other oxides reported in the literature,[14,28−31] and shows the presence of the three stages discussed previously. The stages can be separated by using the derivative of the isotherm: for very small relative pressures (0.02), there is a rapid increase of coverage with the increased pressure. This suggested a high reactivity of the surface at the anhydrous state. Up to about 0.40 of relative pressure, the slope of the isotherm is smaller, and this changes again to a third behavior after that up to higher pressures.

Figure 5 shows the heat of adsorption as a function of relative pressure. For very small pressures, the heat of adsorption is high, being for the first measured coverage (0.4 $H_2O \cdot nm^{-2}$) equal to −158.83 $kJ \cdot mol^{-1}$. To compare with data available in the literature, we will assume that each H_2O generates two OH groups. Digne et al.[32,33] showed by density functional (DFT) calculations that, for the (100) surface, the differential adsorption energy of water for a coverage of 4.3 $OH \cdot nm^{-2}$ is 105 $kJ \cdot mol^{-1}$. For this same coverage, from the data presented

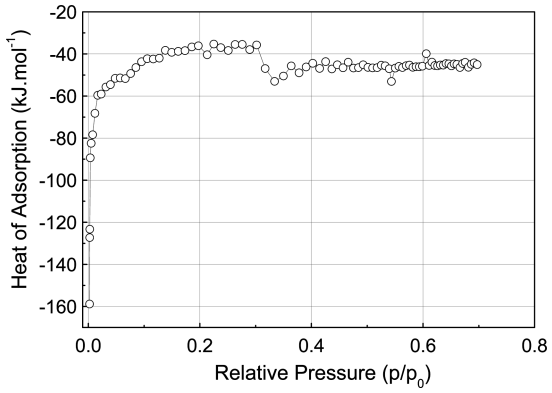

Figure 5. Heat of adsorption as a function of the relative pressure for water adsorbed on gamma-alumina nanoparticles. Data converges to the enthalpy of liquefaction of water after relative pressure above 0.4.

in ref 33, we can estimate the differential adsorption energy as 220 $kJ \cdot mol^{-1}$ for the (110) surface. From our experiments, the differential adsorption energy is ∼116 $kJ \cdot mol^{-1}$ for the 4.3 $OH \cdot nm^{-2}$ coverage (2.15 $H_2O \cdot nm^{-2}$). It is important to note that our data refer to particles rather than isolated surfaces, so it is a combination of the heat effect from adsorption on several exposed planes. It has been shown that alumina particles derived from boehmite typically show a higher fraction of the (110) plane (74%), followed by 16% of (100) and 10% of (111). However, samples prepared by the polymeric precursor method (used in this work) do not evolve from the boehmite, and should not follow the same profile. A quick look at the XRD pattern indicates though that the (440) plane is not as strong with relation to (400) as observed in boehmite derived samples.[34−36] A more quantitative analysis of the particle shape should be done to allow a true comparison of the adsorption energies but is not the goal of this work.

The high adsorption energy for lower coverage reveals a dissociative mode, as detailed elsewhere.[32] The modulus of the heat of adsorption drops fast for higher vapor pressures and finds a first plateau above −44 $kJ \cdot mol^{-1}$, at −35 $kJ \cdot mol^{-1}$. A common mistake when analyzing data from similar adsorption experiments is to assume that this plateau is actually already the expected −44 $kJ \cdot mol^{-1}$, and the observed deviation is originated from experimental issues.[37,38] After several repetitions under controlled conditions, we discovered that this energy is actually real, and the fact that the heat is above −44 $kJ \cdot mol^{-1}$ only suggests there are a few hydrophobic sites on the studied surface, as discussed by Bolis et al.[27] With increasing pressure, the heat of adsorption increases in modulus again for relative humidity higher than 40%, and stays fairly constant at ∼ −44 $kJ \cdot mol^{-1}$, finally revealing the liquid-like state. As expected from the theoretical description, this state appears exactly when the adsorption isotherm shows an inflection, as seen in Figure 4. The consistency between the heats of adsorption, the adsorption isotherm, and the water structures reported previously is remarkable, indicating that the surface energy of the system at that point is most likely 0.072 $J \cdot m^{-2}$ and encouraging the use of eq 6 to calculate the surface energies at the different coverages.

To use it, one needs to identify the precise coverage where the surface starts to behave unambiguously as a liquid. Both heat of adsorption and adsorption isotherm provide an indication on the critical coverage, but to quantify that number, we looked for the coverage where the second derivative of the

dx.doi.org/10.1021/jp309319j | J. Phys. Chem. C 2012, 116, 24726−24733

adsorption isotherm curve is zero. This coverage is 31.8 OH·nm^{-2} for gamma-alumina. With this, one can apply eq 6 to this coverage, setting γ^S as 0.072 J·m^{-2}. One can then use the total coverage up to that point and the integral of the heats of adsorption to determine the anhydrous surface energy, which is 1.54 J·m^{-2}. Table 1 shows how this number compares to those

Table 1. Anhydrous Surface Energies in J·m^{-2} Determined by Using Water Adsorption Experiments and Literature Data from Both Drop Solution Calorimetry and Theoretical Calculations as Cited[a]

	this work	literature
γ-Al_2O_3	1.54	1.53;[13] 1.67;[12] 0.97$^{(100)}$; 1.54$^{(110)}$; 1.97$^{(111)}$ [33]

[a]Superscripts in parentheses are the respective surface planes.

available in the literature for gamma-alumina from both experimental approaches (high temperature oxide melt solution calorimetry) and computational. As observed, the method provides a number within the acceptable energies for this material. This number is very consistent with those reported previously for gamma-alumina prepared by exactly the same synthesis technique.[13] From an experimental point of view, though, this number is more reliable than those proposed by melt solution calorimetry, since a single sample is used for the measurement. The errors involved in our data will be mostly related to the uncertainties on the measurement of the relative pressures (<0.15%), the error of surface area measurement (2%), and that from the calorimetric measurements themselves. For this last one, repeated experiments were performed with similar samples and conditions, and the difference between samples was ~0.05 J·m^{-2} on the calculated surface energies (both anhydrous and hydrous). This is considerably better than the error reported on surface energies of oxides determined from high temperature melt solution calorimetry.

Figure 6 shows the calculated surface energies at room temperature from our work as a function of the surface

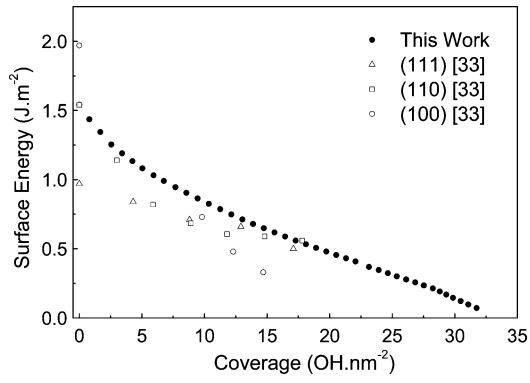

Figure 6. Solid symbols are the surface energies for gamma-alumina as a function of water coverage determined by the proposed water adsorption microcalorimetry study. The open symbols are calculated using DFT from ref 33.

coverage (solid symbols). Numbers by DFT calculated for 400 K are also plotted for comparison (open symbols). The experimental data show the expected increase in the surface energy with decreasing coverage. The energy is 0.072 J·m^{-2} for 31.8 OH·nm^{-2} and increases up to 1.54 J·m^{-2} for the anhydrous conditions. The shape of the increasing curve is consistent with those reported from DFT, showing a steeper increase of the surface energy at lower coverage. The anhydrous number from our work lies within those calculated for the planes (100), (110), and (111). However, the experimental energies estimated for nonzero coverage are systematically higher than the DFT calculations. This can be attributed to several things, such as assumptions in DFT, morphological effects, etc., but we believe it is related to a particularity of the water coverage term definition. In this work, we assumed that every absorbed water molecule generates 2 OH·nm^{-2}. This is similar to what Digne et al. performed in their calculations, but from an experimental point of view, this dissociative picture may not hold true for the entire adsorption process. This is because nondissociative behavior may compete with dissociative behavior even at relatively low coverage, since different surfaces are available and the morphology of the surfaces is also affecting the adsorption behavior. Obviously, the nondissociative behavior is more critical for high coverage degrees, as pointed out in the three-stage adsorption model described previously.

4. DISCUSSION

The acquired data is representative of the tested sample, and shows for the first time the possibility of assessing the anhydrous and hydrated (at different water coverages) surface energies of alumina and potentially other oxides. The data presented for alumina show a relationship between the water adsorption on the oxide surface and the surface energy variation; i.e., when comparing the adsorption data in Figure 4 with the surface energy curve in Figure 6, one can make a parallel about the reactivity of the surface and its interaction with water molecules. Figure 7 shows both surface energy and

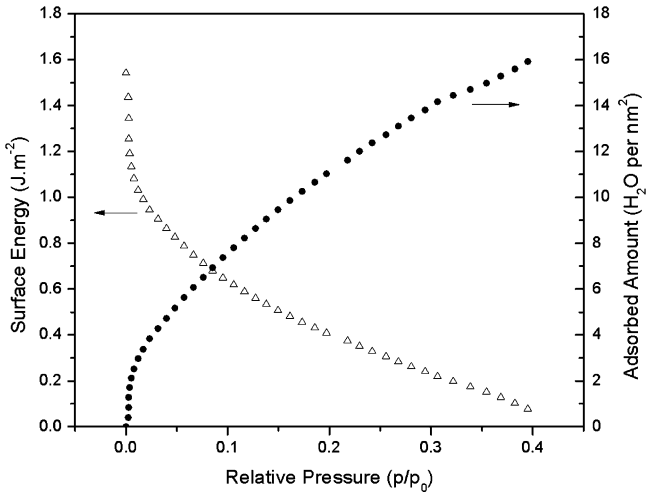

Figure 7. Surface water coverage and surface energy of gamma-alumina as a function of relative pressure of water vapor. Similar behavior suggests a close relationship between these parameters.

coverage as a function of relative pressure for a direct comparison. At low coverage, there is a large surface energy change with adsorption, and this is associated with a high amount of absorbed water even with very low relative pressure differences (p/p_0 < 0.01), and a consequent high heat of adsorption per molecule. At this stage, we can expect a dissociative behavior of water adsorption, and the heat of

dx.doi.org/10.1021/jp309319j | J. Phys. Chem. C 2012, 116, 24726−24733

adsorption is consistent with this picture. As the surface is "cured" by the water adsorption (using the term introduced by McHale et al. in ref 12), the slopes of surface energy variation and adsorption amount decrease in modulus. This is also associated with a decrease in the heat of adsorption, suggesting that the adsorption mode is changing as the highly reactive (hydrophilic) sites are getting occupied. The fact that the heat of adsorption is still higher in modulus (more negative) than 44 $kJ{\cdot}mol^{-1}$ suggests it is still a (mostly) dissociative behavior (as we are dealing with average energies, it might be possible to have also nondissociative behaviors taking place). This stage follows a typical *one-surface* adsorption behavior and can be described by the Gibbs adsorption isotherm, and for gamma-alumina is shown to go up to $p/p_0 \sim 0.3$. The surface energy at this point decays continuously, as expected and consistently with the heat of adsorption.

After occupying most free surface sites (roughly three monolayers assuming a H_2O molecule to occupy 25×10^{-20} m^2 [14]), at $0.3 < p/p_0 < 0.4$, the water molecules start to pile up, forming a thick layer over the surface (consistently with the macroscopic description reported elsewhere[20]). The combination of adsorption and heat of adsorption allows us to actually define this transient state, which is about ~3.6 $OH{\cdot}nm^{-2}$ thick (about a monolayer). After the transient state, the heat of adsorption is getting closer to heat of liquefaction, and the surface energy is closer to the liquid state. This is reflected on the adsorption behavior which clearly shows a plateau around -44 $kJ{\cdot}mol^{-1}$. At this point, the majority of the molecules are being physisorbed and will continue to do so at even higher pressures ($p/p_0 > 0.4$). The surface energy for higher pressures will be that of liquid water.

This picture is very consistent with the adsorption behavior presented in Figure 1 for SiO_2 data,[24] with similar coverage (in terms of monolayers) but different relative pressures. This suggests a similar configuration of the water molecules on the surface but a higher affinity of gamma-alumina for them. The present work represents the first time one can experimentally correlate the coverage model with measured heats of adsorption and surface energies, connecting the molecular configuration perspective with the macroscopic description of the problem.

5. CONCLUSIONS

A method for the direct measurement of the surface energy of nanocrystalline and bulk oxides was described on the basis of water adsorption experiments. The method is based on the reversibility of the water adsorption on the surface of the nanoparticles, such that, if the heat exchange is measured during the adsorption of water on an anhydrous surface, the data can be used to calculate the surface energy at the different water coverage states. The method was successfully used to derive the surface energies of gamma-alumina which was very consistent with available data in the literature. Along with the surface energy calculation, the combination of data generated provided unique insights on the water adsorption behavior on gamma-alumina. We could depict three adsorption stages, one when most adsorption is dissociative and the surface is composed of a single interface, a second transient state, and a final where water is physisorbed and forming a thick film on the top of each particle. It is shown that the water adsorption causes a "curing" effect on the surface energy, systematically decreasing its energy. The adsorption curve shows an interesting connection to the variation of the surface energy, and because of that, it can provide some indirect evidence of the surface energy behavior.

The proposed method for assessing the surface energy shows a great potential for application in technological fields since a single set of samples is required. The results are representative of the specific sample being experimented though, and different samples, even of the same composition, with distinct exposed surfaces due to processing or particle shape are expected to have slightly different surface energies. A characterization of the sample prior to the analysis is therefore very important to understand the obtained values in terms of surface planes, and surface structures.

AUTHOR INFORMATION

Corresponding Author

*E-mail: rhrcastro@ucdavis.edu. Fax: (530) 752-9307. Phone: (530) 752-3724.

Notes

The authors declare no competing financial interest.

ACKNOWLEDGMENTS

The author would like to thank NSF DMR CAREER 1055504 for financing the development of this method. Professor Douglas Gouvêa is thanked for fruitful discussions. D.V.Q. was supported by the US Department of Energy, Office of Basic Energy Sciences.

REFERENCES

(1) Zhao, Z. J.; Meza, J. C.; Van Hove, M. *J. Phys.: Condens. Matter* **2006**, *18*, 8693−8706.
(2) Navrotsky, A. Thermochemistry of nanomaterials. In *Reviews in Mineralogy and Geochemistry: Nanoparticles and the Environment*; Banfield, J. F., Navrotsky, A., Eds.; Mineralogical Society of America and the Geochemical Society: Washington, DC, 2001; Vol. *44*; pp 73−103.
(3) Hill, T. L. *Nano Lett.* **2001**, *1*, 111−112.
(4) Hill, T. L. *Nano Lett.* **2001**, *1*, 159−160.
(5) Rusanov, A. I. *Russ. J. Phys. Chem.* **2003**, *77*, 1558−1563.
(6) Yun, G.; Park, H. S. *Comput. Methods Appl. Mech. Eng.* **2008**, *197*, 3337−3350.
(7) Castro, R. H. R.; Marcos, P. J. B.; Lorriaux, A.; Steil, M. C.; Gengembre, L.; Roussel, P.; Gouvea, D. *Chem. Mater.* **2008**, *20*, 3505−3511.
(8) Kendall, K.; Alford, N. M.; Birchall, J. D. *Nature* **1987**, *325*, 794−796.
(9) Bikerman, J. J. *Metall.* **1975**, *29*, 597−598.
(10) Argon, A. S. *Phys. Status Solidi* **1965**, *12*, K121−K125.
(11) Triantafyllou, G.; Angelopoulos, G. N.; Nikolopoulos, P. *J. Mater. Sci.* **2010**, *45*, 2015−2022.
(12) McHale, J. M.; Auroux, A.; Perrotta, A. J.; Navrotsky, A. *Science* **1997**, *277*, 788−791.
(13) Castro, R. H. R.; Ushakov, S. V.; Gengembre, L.; Gouvea, D.; Navrotsky, A. *Chem. Mater.* **2006**, *18*, 1867−1872.
(14) Ushakov, S. V.; Navrotsky, A. *Appl. Phys. Lett.* **2005**, *87*, No. 164103.
(15) Zhang, P.; Xu, F.; Navrotsky, A.; Lee, J. S.; Kim, S.; Liu, J. *Chem. Mater.* **2007**, *19*, 5687−5693.
(16) Hummer, D. R.; Kubicki, J. D.; Kent, P. R. C.; Post, J. E.; Heaney, P. J. *J. Phys. Chem. C* **2009**, *113*, 4240−4245.
(17) Castro, R. H. R.; Wang, B. *J. Am. Ceram. Soc.* **2010**, *94*, 918−924.
(18) Xu, F.; Zhang, P.; Navrotsky, A.; Yuan, Z.-Y.; Ren, T.-Z.; Halasa, M.; Su, B.-L. *Chem. Mater.* **2007**, *19*, 5680−5686.
(19) Bangham, D. H.; Razouk, R. I. *Trans. Faraday Soc.* **1937**, *33*, 1459−1463.

(20) Schlangen, L. J. M.; Koopal, L. K.; Stuart, M. A. C.; Lyklema, J. *Colloids Surf., A* **1994**, *89*, 157−167.
(21) Churaev, N. V.; Setzer, M. J.; Adolphs, J. *J. Colloid Interface Sci.* **1998**, *197*, 327−333.
(22) Fang, X. H.; Li, B. Q.; Chernyshova, I. V.; Somasundaran, P. *J. Phys. Chem. C* **2010**, *114*, 15473−15477.
(23) Adamson, A. W. *J. Colloid Interface Sci.* **1968**, *27*, 180−187.
(24) Asay, D. B.; Kim, S. H. *J. Phys. Chem. B* **2005**, *109*, 16760−16763.
(25) Al-Abadleh, H. A.; Grassian, V. H. *Langmuir* **2003**, *19*, 341−347.
(26) Hauyn, S.; Tran, T.; Ushakov, S. V.; Thron, A. M.; van Benthem, K.; Navrotsky, A.; Castro, R. H. R. *J. Phys. Chem. C* **2011**, *115*, 23929−23935.
(27) Bolis, V.; Fubini, B.; Marchese, L.; Martra, G.; Costa, D. *J. Chem. Soc., Faraday Trans.* **1991**, *87*, 497−505.
(28) Ma, Y.; Castro, R. H. R.; Zhou, W.; Navrotsky, A. *J. Mater. Res.* **2011**, *26*, 848−853.
(29) Navrotsky, A.; Ma, C.; Lilova, K.; Birkner, N. *Science* **2010**, *330*, 199−201.
(30) Ushakov, S. V.; Dalalo, N.; Navrotsky, A. *Geochim. Cosmochim. Acta* **2005**, *69*, A485−A485.
(31) Mazeina, L.; Deore, S.; Navrotsky, A. *Chem. Mater.* **2006**, *18*, 1830−1838.
(32) Digne, M.; Sautet, P.; Raybaud, P.; Euzen, P.; Toulhoat, H. *J. Catal.* **2002**, *211*, 1−5.
(33) Digne, M.; Sautet, P.; Raybaud, P.; Euzen, P.; Toulhoat, H. *J. Catal.* **2004**, *226*, 54−68.
(34) Zhou, R. S.; Snyder, R. L. *Acta Crystallogr., Sect. B: Struct. Sci.* **1991**, *47*, 617−630.
(35) Alex, T. C.; Kumar, C. S.; Kailath, A. J.; Kumar, R.; Roy, S. K.; Mehrotra, S. P. *Metall. Mater. Trans. B* **2011**, *42*, 592−603.
(36) Ghamsari, M. S.; Mahzar, Z. A. S.; Radiman, S.; Hamid, A. M. A.; Khalilabad, S. R. *Mater. Lett.* **2012**, *72*, 32−35.
(37) Ma, C.; Navrotsky, A. *Chem. Mater.* **2012**, *24*, 2311−2315.
(38) Radha, A. V.; Bomati-Miguel, O.; Ushakov, S. V.; Navrotsky, A.; Tartaj, P. *J. Am. Ceram. Soc.* **2009**, *92*, 133−140.